Optical Readout of the Quantum Collective Motion of an Array of Atomic Ensembles

Thierry Botter,[1,*] Daniel W. C. Brooks,[1] Sydney Schreppler,[1] Nathan Brahms,[1] and Dan M. Stamper-Kurn[1,2,†]

[1]*Department of Physics, University of California, Berkeley, California 94720, USA*

[2]*Materials Sciences Division, Lawrence Berkeley National Laboratory, Berkeley, California 94720, USA*

(Received 18 October 2012; published 8 April 2013)

We create an ultracold-atom-based cavity optomechanical system in which the center-of-mass modes of motion of as many as six distinguishable atomic ensembles are prepared and optically detected near their ground states. We demonstrate that the collective motional state of one atomic ensemble can be selectively addressed while preserving neighboring ensembles near their ground states to better than 95% per excitation quantum. We also show that our system offers nanometer-scale spatial resolution of each atomic ensemble via optomechanical imaging. This technique enables the *in situ* parallel sensing of potential landscapes, a capability relevant to active research areas of atomic physics and force-field detection in optomechanics.

DOI: 10.1103/PhysRevLett.110.153001 PACS numbers: 37.10.Vz, 03.65.−w, 42.50.−p, 42.65.−k

Cavity-enhanced interactions between light and the motion of a mechanical element form a new framework for quantum-sensitive displacement measurements [1,2]; the generation of nonclassical light [3]; the storage [4,5], control [6,7], and transduction [8,9] of quantum information; and the optical cooling of an oscillator to its motional ground state [10,11]. To date, research efforts have focused almost exclusively on coupling a single mechanical element to light.

Cavity optomechanics with multiple moveable elements promises new possibilities, including optomechanical networks for quantum information processing [9,12,13], the entanglement of macroscopic quantum systems [14,15], and experimental studies of light-mediated oscillator-oscillator interactions [16,17]. Recently, researchers have begun exploring multioscillator optomechanics, employing pairs of nanomechanical oscillators [18–21]. These studies have explored coupling of the mechanical modes via a shared evanescent optical field or, in the case of Ref. [21], a shared microwave-frequency resonator. Certain classical effects were demonstrated, including the synchronization of motion and the hybridization of modes into optically bright and dark states.

In this work, we extend these results by observing two distinctly quantum-mechanical features of an atom-based realization of cavity optomechanics in which several distinguishable atomic ensembles, prepared near their motional ground states, are arrayed within the same optical resonator; the center-of-mass motion of each ensemble forms an effective moving object that can be optomechanically sensed. First, we demonstrate that the near-ground-state collective motion of as many as six atomic ensembles can be simultaneously measured with quantum-limited sensitivity. Second, we show that the state of a selected center-of-mass mode can be changed without disturbing the near quantum motion of neighboring collective modes.

Previous experiments investigating cavity optomechanics through the motion of atomic ensembles have used gases trapped within a single-color standing wave of light, formed by driving a Fabry-Pérot cavity on one of its TEM_{00} resonances [22–24]. In such a potential, atoms at every lattice site oscillate at the same mechanical frequency. This mechanical degeneracy allows the motion of the entire array of trapped ensembles to be treated as that of a single mechanical element.

Here, instead, two optical trap beams of distinct colors, labeled A and B, each resonant with a separate TEM_{00} mode, are injected into a Fabry-Pérot cavity. Neglecting the variation of the cavity-field intensity in the directions transverse to the cavity axis, the resulting one-dimensional optical potential is of the form

$$U = U_A \sin^2(k_A z) + U_B \sin^2(k_B z), \tag{1}$$

where U and k are the optical potential trap depth and wave number, respectively, and z refers to the spatial location. In this superlattice, the potential curvature and, hence, the mechanical oscillation frequency of trapped atoms vary among neighboring lattice sites. Upon distributing atoms among several adjacent lattice sites, the collective center-of-mass vibrations of the population at each occupied site represent distinct mechanical objects that can interact optomechanically with a cavity-probe field.

In our experiment, a microfabricated atom chip produces an ultracold gas of ^{87}Rb atoms that is magnetically trapped within the mode volume of a Fabry-Pérot optical cavity of half-linewidth $\kappa = 2\pi \times 1.82$ MHz [23]. The initial position of the atomic gas along the cavity axis z_a is controlled by varying the magnetic trap's parameters. Tunable radio-frequency-induced evaporation allows us to reduce the atom number and also the spatial extent of the magnetically trapped atoms by lowering their temperature. The remaining atoms are then transferred from the magnetic trap to the optical superlattice formed by lattice

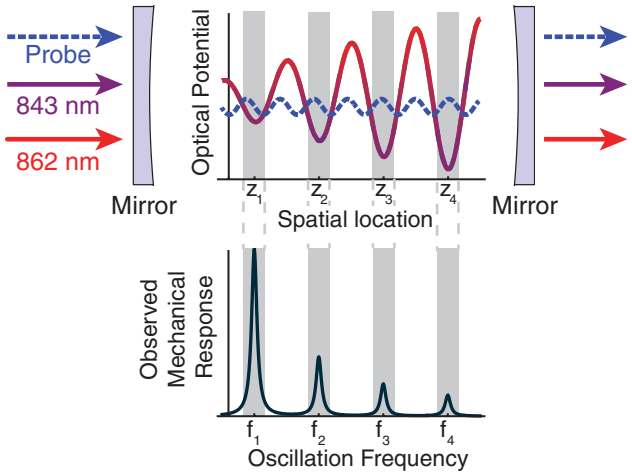

FIG. 1 (color). Experiment schematic: Superlattice potential. Three light beams are injected into an optical cavity (mirrors—gray areas): the probe (dashed blue arrow) and lattice beams A (solid red arrow) and B (solid purple arrow). The atoms inserted into the cavity are trapped in potential minima of the superlattice formed by spatial beats between each lattice beam's standing-wave optical potential (red-purple gradient). The dissimilar wavelengths of lattice beams A and B (862 and 843 nm, respectively) cause atoms at neighboring lattice sites to resonate at distinct frequencies. Their motion is detected via optomechanical interactions with the probe's standing-wave intensity (intracavity, dashed blue). Since each potential minimum overlaps with a different probe-intensity gradient, the observed response varies in amplitude among neighboring lattice sites.

beams A [$k_A = 2\pi/(862\text{ nm})$] and B [$k_B = 2\pi/(843\text{ nm})$] (Fig. 1). The lattice depths $U_{A,B}$ are chosen so that the mechanical resonance frequencies for each of the single-color standing waves that form the superlattice are given as $\omega_{A,B} = \sqrt{2k_{A,B}^2 U_{A,B}/m} = 2\pi \times (127, 128\text{ kHz})$, where m is the atomic mass (see the Supplemental Material [25], Fig. S.1).

Information about the motion of the resulting array of ensembles is then extracted via optomechanical interactions with a third light beam, the probe beam, resonant with a separate TEM_{00} cavity mode and detuned $\Delta_{\text{ca}} = -40$ GHz from the atomic D2 transition [$k_p = 2\pi/(780\text{ nm})$]. At this detuning, atoms act primarily as a refractive medium with a single-atom cavity-QED coupling rate of $g_0 = 2\pi \times 13.1$ MHz. The center-of-mass displacement $\hat{Z}_i$ of each atomic ensemble from its trap center z_i consequently shifts the cavity resonance frequency ω_c, and hence the probe's phase, by an amount

$$\Delta\omega_c = \hat{Z}_i \frac{N_i k_p g_0^2}{\Delta_{\text{ca}}} \sin(2k_p z_i), \tag{2}$$

where k_p is the probe wave number, N_i is the number of atoms in each ensemble, and $\sin(2k_p z_i)$ quantifies the local probe-intensity gradient [22,26]. The temporal evolution of the motion of each ensemble is thus imprinted on the cavity emission spectrum. Since the different ensembles oscillate mechanically at distinct frequencies, the record of each ensemble's motion can be distinguished. The probe light transmitted through the cavity is detected using a balanced heterodyne receiver with an overall efficiency of 0.13 ± 0.02 for detecting cavity photons. Atoms are then released from the optical trap, and the cavity probe light is again measured. This second measurement is subtracted from the first to identify and eliminate technical noise. To avoid excessive probe-induced heating of the atomic gas, data recordings are limited to 10 ms.

We begin by characterizing the distribution of potential minima of the optical superlattice. In a single experimental cycle, a small cloud of $\sim$1000 atoms is loaded into the superlattice at an initial position z_a chosen within a range spanning a full superlattice period $\pi/(k_A - k_B) = 19.4\,\mu$m. The cavity is then probed at a light intensity corresponding to an average intracavity photon number of 2.9. From the recorded optical heterodyne signal, we extract the spectrum of motional sidebands imparted by the atomic motion, characterizing the mechanical structure of the intracavity atomic ensembles.

These phase-quadrature power spectra ($S_{\text{het}}^{(\pi/2)}(\omega)$ in the Supplemental Material [25]), shown in Fig. 2(a), display a set of discrete mechanical resonances generated by atoms trapped at different locations within the superlattice. Indeed, the relation between z_a and the observed mechanical resonances provides a detailed spatial mapping of the superlattice potential minima, one which agrees closely with the predicted form of the potential. The motional sidebands also vary strongly in their strength, owing to the site-to-site variation in the linear optomechanical coupling strength [Eq. (2)]. The probe-light intensity at each superlattice trap site can be inferred from the mean shift of the cavity resonance frequency by atoms loaded into that site [Fig. 2(b)]. As expected, strong motional sidebands are observed for atoms placed where this intensity shows large gradients.

The resolution with which the center location of each potential minimum can be imaged depends on the spacing between adjacent lattice sites, $a = 420$ nm, the initial atomic cloud's spatial full width at half-maximum (FWHM) σ_w and the precision with which z_a can be controlled, parameterized by the FWHM σ_{z_a}. For infinitely narrow initial atomic distributions with arbitrarily precise initial locations, atoms inserted within $\pm a/2$ of a potential minimum will be trapped at the same location, yielding an effective spatial resolution of a. For initial atomic clouds of FWHM $\sigma_{\text{tot}} \gg a$, due to either large σ_w or randomly fluctuating z_a, each populated lattice site's center location will be measured with a resolution of $\sigma_{\text{tot}} = \sqrt{\sigma_w^2 + \sigma_{z_a}^2}$. For the region considered in Fig. 2(c), the spatial resolution limit is 420 nm, i.e., at the single lattice site limit.

Having characterized the optical superlattice, we construct an array of distinguishable collective motional modes by inserting a spatially broad Gaussian distribution

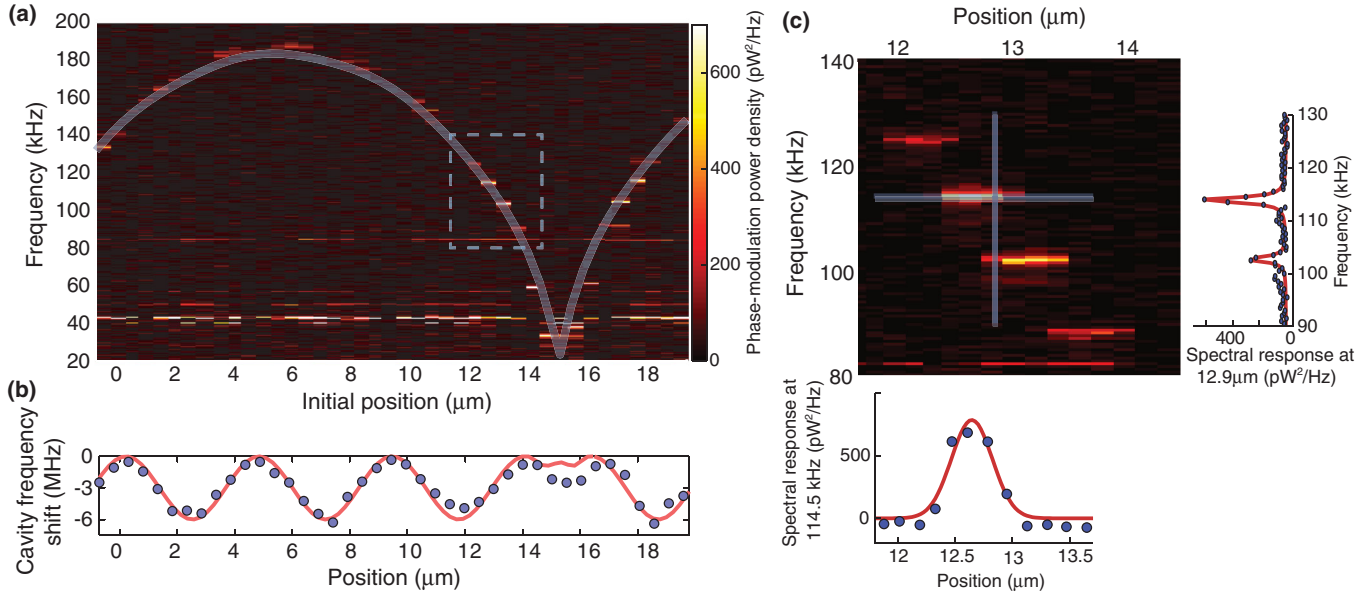

FIG. 2 (color). Distribution of mechanical resonances along the superlattice. (a) Phase-quadrature power density as a function of frequency and loading position of the initial atomic sample, z_a, measured from a point within the middle of the cavity. Discrete mechanical responses appear as bright pixels. They closely follow the transparent gray curve, which interpolates between the expected discrete mechanical resonances. Residual technical noise appears as horizontal bands in the figure (e.g., near 40 kHz). (b) Measured shifts (purple dots) in the probe's cavity resonance are due to dispersive probe-atom coupling at each recorded superlattice position, overlaid with the modeled distribution of cavity frequency shifts (solid red line). Regions of maximum gradient are correlated with the brightest responses in (a). (c) Mechanical responses measured with finer steps between loading positions [within the dashed box in (a)]. Measured spectral responses across a selected frequency and position (transparent gray lines) are shown adjacent to the central figure (data, purple dots; fits, solid red lines). The fits yield a spatial and spectral resolutions of $\sigma_{\mathrm{tot}} = 0.42 \pm 0.05$ μm and $\Gamma = 2\pi \times (1.2 \pm 0.1)$ kHz, respectively, for the oscillator at frequency $\omega = 2\pi \times 114.5$ kHz.

of atoms ($\sigma_{\mathrm{tot}} \sim 3.1$ μm) at location 11.7 μm [see Figs. 2(a) and 2(c)], where the frequency difference between neighboring mechanical resonances exceeds the mechanical resonance frequency widths Γ (FWHM). Atoms are transfered to the many lattice sites overlapping with the initial cloud, resulting in several distinguishable atomic ensembles composed of 400 to 800 atoms each. We record the distribution of motional sidebands imprinted on the cavity-resonant probe photon spectrum $\bar{n}(\omega)$ (see the Supplemental Material [25], Sec. S.1). As many as six distinct center-of-mass modes are observed (Fig. 3). In fact, for these data, atoms occupy at least eight neighboring sites of the superlattice, but two sites are only weakly detected due to minimal linear optomechanical coupling at their locations.

We demonstrate the quantum nature of these collective motional modes using a parallel measurement of their Stokes emission asymmetry [26,27]. The asymmetry between the rate of red-detuned (Stokes) $\dot{\bar{n}}_i^{(r)}$ and blue-detuned (anti-Stokes) $\dot{\bar{n}}_i^{(b)}$ scattered photons, near the mechanical frequency of site i, reveals the center-of-mass mode to be near its quantum-mechanical ground state. That is, when the cavity is probed on resonance, this asymmetry quantifies the mean phonon occupation to be $\bar{\nu}_i = \dot{\bar{n}}_i^{(b)}/(\dot{\bar{n}}_i^{(r)} - \dot{\bar{n}}_i^{(b)})$. Mean energy inputs from the atoms' average thermal occupation ($\bar{\nu}_i^{(\mathrm{th})}$) and from optomechanical interactions with the probe ($\bar{\nu}_i^{(\mathrm{ba})}$), in equilibrium with mean energy decay via mechanical damping, sum to give a total phonon occupation number of $\bar{\nu}_i = \bar{\nu}_i^{(\mathrm{th})} + \bar{\nu}_i^{(\mathrm{ba})}$. The measured occupation numbers in our six-ensemble array range from 0.9 to 2.2 (Fig. 3). These occupation numbers include the perturbative action of the probe and hence constitute upper bounds on each ensemble's native motional state $\bar{\nu}_i^{(\mathrm{th})}$. As highlighted by the inset of Fig. 3, by varying the spatial extent of the initial atomic cloud, the number of distinct atomic ensembles can be controllably tuned from one to six.

In addition, we demonstrate that one targeted collective atomic mode can be driven coherently while preserving the near quantum motion of neighboring center-of-mass modes. Ensembles α and β (Fig. 3) are prepared with ~750 atoms each. We apply a nearly equal force modulation to both ensembles by temporarily modulating U_B but we tune the modulation frequency to coincide with one targeted ensemble's mechanical resonance frequency. Each collective mode's squared displacement, and hence its mechanical energy, is mapped onto the probe's phase-quadrature power density, which we record at the cavity output (see the Supplemental Material [25], Sec. S.2).

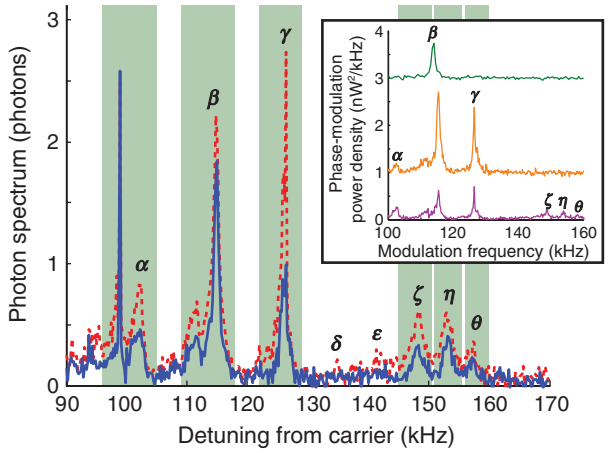

FIG. 3 (color). Stokes (dashed red curve) and anti-Stokes (solid blue curve) sideband spectra of light exiting the cavity as a function of detuning from the probe carrier frequency. Atoms are loaded into eight neighboring lattice sites, labeled sequentially by position (Greek letters). Only six motional sidebands pairs are visible because two atomic ensembles (δ and ϵ) are positioned where the linear optomechanical response is minimal. Phonon occupations are obtained from the integrated Stokes and anti-Stokes fluorescence in narrow frequency bands around each mechanical resonance (light-green shaded areas): $\nu_\alpha = 1.8 \pm 0.2$, $\nu_\beta = 2.2 \pm 0.2$, $\nu_\gamma = 1.0 \pm 0.1$, $\nu_\zeta = 0.9 \pm 0.1$, $\nu_\eta = 1.3 \pm 0.2$, and $\nu_\theta = 1.8 \pm 0.4$. The narrow response at 99 kHz is an optomechanically amplified technical noise spike on the probe. (Inset) Demonstration of experimental control over the number of mechanical modes. The initial atomic clouds of narrow (top green curve), medium (middle orange curve), and wide (bottom purple curve) spatial extents are prepared to produce arrays of one, three, and six atomic ensembles, respectively. The traces are offset for clarity.

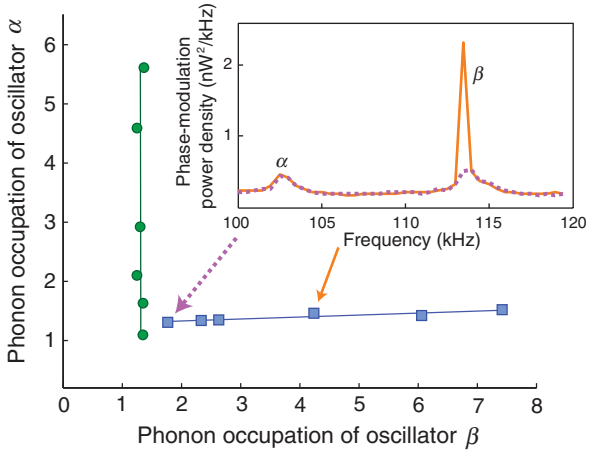

FIG. 4 (color). Selective addressing of a single atomic ensemble. Energy is deposited into ensembles α (green dots) and β (blue squares), respectively, by coherently modulating the intensity of lattice beam B. The points correspond to the measured center-of-mass phonon occupation under different modulation strengths of U_B. The lines are fits to the data. From the slopes and their uncertainties, the phonon occupation of the undriven site increases by less than 0.04 (blue line and squares) and 0.05 (green line and dots), within a 97% confidence interval, for every phonon added to the driven site. (Inset) Measured phase-quadrature power density for two distinct drives at ω_β (dashed purple and orange solid curves). The arrows point to the corresponding data points.

Figure 4 shows the measured simultaneous mean phonon occupation of both ensembles' center-of-mass motion. The plotted occupations include energy provided by the drive in addition to the thermal and probe-induced phonon occupation. Linear fits to both series of drives indicate a base phonon occupation of 1.3 for each oscillator. Moreover, for each quantum of collective motion added to ensemble α or β, fewer than 0.05 and 0.04 phonons are added to the other ensemble, respectively. Each ensemble is therefore isolated from its neighbor by at least 95% per added mechanical quantum.

An important application of cavity optomechanics is precise force sensing [28]. Having an array of mechanically distinct oscillators allows one to make such force measurements simultaneously at many spatial locations, using frequency multiplexing to read out the array of force sensors with a single cavity-optical output. This can serve as a means to measure minute and sharply varying force fields, such as short-range gravitational forces and Casimir-Polder forces. Additionally, the use of optomechanics to characterize our superlattice potential (Fig. 2), a method which could be termed "mechanical resonance imaging," can be broadly applied to directly measure any potential landscape. Sub-wavelength-scale potential variations could be resolved, given our system's nanometer-scale control over the initial atomic cloud's size and location. This technique has direct relevance to the many-body physics of quantum interactions [29], Anderson localization [30,31], and studies of particle dynamics in different optical superlattice structures [32].

This work was supported by the AFOSR and the NSF. S. S. acknowledges support from NDSEG.

*tbotter@berkeley.edu
†dmsk@berkeley.edu

[1] J. D. Teufel, T. Donner, M. A. Castellanos-Beltran, J. W. Harlow, and K. W. Lehnert, Nat. Nanotechnol. **4**, 820 (2009).
[2] G. Anetsberger, O. Arcizet, Q. P. Unterreithmeier, R. Rivire, A. Schliesser, E. M. Weig, J. P. Kotthaus, and T. J. Kippenberg, Nat. Phys. **5**, 909 (2009).
[3] D. W. C. Brooks, T. Botter, S. Schreppler, T. P. Purdy, N. Brahms, and D. M. Stamper-Kurn, Nature (London) **488**, 476 (2012).
[4] S. Weis, R. Rivire, S. Delglise, E. Gavartin, O. Arcizet, A. Schliesser, and T. J. Kippenberg, Science **330**, 1520 (2010).

[5] A. H. Safavi-Naeini, T. P. M. Alegre, J. Chan, M. Eichenfield, M. Winger, Q. Lin, J. T. Hill, D. E. Chang, and O. Painter, Nature (London) **472**, 69 (2011).
[6] J. Rosenberg, Q. Lin, and O. Painter, Nat. Photonics **3**, 478 (2009).
[7] D. van Thourhout and J. Roels, Nat. Photonics **4**, 211 (2010).
[8] A. D. O'Connell, M. Hofheinz, M. Ansmann, R. C. Bialczak, M. Lenander, E. Lucero, M. Neeley, D. Sank, H. Wang, M. Weides, J. Wenner, J. M. Martinis, and A. N. Cleland, Nature (London) **464**, 697 (2010).
[9] D. E. Chang, A. H. Safavi-Naeini, M. Hafezi, and O. Painter, New J. Phys. **13**, 023003 (2011).
[10] J. D. Teufel, T. Donner, D. Li, J. W. Harlow, M. S. Allman, K. Cicak, A. J. Sirois, J. D. Whittaker, K. W. Lehnert, and R. W. Simmonds, Nature (London) **475**, 359 (2011).
[11] J. Chan, T. P. M. Alegre, A. H. Safavi-Naeini, J. T. Hill, A. Krause, S. Groblacher, M. Aspelmeyer, and O. Painter, Nature (London) **478**, 89 (2011).
[12] M. Schmidt, M. Ludwig, and F. Marquardt, New J. Phys. **14**, 125005 (2012).
[13] K. Stannigel, P. Komar, S. J. M. Habraken, S. D. Bennett, M. D. Lukin, P. Zoller, and P. Rabl, Phys. Rev. Lett. **109**, 013603 (2012).
[14] S. Mancini, V. Giovannetti, D. Vitali, and P. Tombesi, Phys. Rev. Lett. **88**, 120401 (2002).
[15] M. Pinard, A. Dantan, D. Vitali, O. Arcizet, T. Briant, and A. Heidmann, Europhys. Lett. **72**, 747 (2005).
[16] M. Ludwig and F. Marquardt, arXiv:1208.0327v1.
[17] A. Xuereb, C. Genes, and A. Dantan, Phys. Rev. Lett. **109**, 223601 (2012).
[18] X. Jiang, Q. Lin, J. Rosenberg, K. Vahala, and O. Painter, Opt. Express **17**, 20 911 (2009).
[19] Q. Lin, J. Rosenberg, D. Chang, R. Camacho, M. Eichenfield, K. J. Vahala, and O. Painter, Nat. Photonics **4**, 236 (2010).
[20] M. Zhang, G. S. Wiederhecker, S. Manipatruni, A. Barnard, P. McEuen, and M. Lipson, Phys. Rev. Lett. **109**, 233906 (2012).
[21] F. Massel, S. U. Cho, J.-M. Pirkkalainen, P. J. Hakonen, T. T. Heikkilä, and M. A. Sillanpää, Nat. Commun. **3**, 987 (2012).
[22] F. Brennecke, S. Ritter, T. Donner, and T. Esslinger, Science **322**, 235 (2008).
[23] T. P. Purdy, D. W. C. Brooks, T. Botter, N. Brahms, Z.-Y. Ma, and D. M. Stamper-Kurn, Phys. Rev. Lett. **105**, 133602 (2010).
[24] M. H. Schleier-Smith, I. D. Leroux, H. Zhang, M. A. Van Camp, and V. Vuletić, Phys. Rev. Lett. **107**, 143005 (2011).
[25] See Supplemental Material at http://link.aps.org/supplemental/10.1103/PhysRevLett.110.153001 for [brief decription].
[26] N. Brahms, T. Botter, S. Schreppler, D. W. C. Brooks, and D. M. Stamper-Kurn, Phys. Rev. Lett. **108**, 133601 (2012).
[27] A. H. Safavi-Naeini, J. Chan, J. T. Hill, T. P. M. Alegre, A. Krause, and O. Painter, Phys. Rev. Lett. **108**, 033602 (2012).
[28] H. J. Mamin and D. Rugar, Appl. Phys. Lett. **79**, 3358 (2001).
[29] J. E. Lye, L. Fallani, M. Modugno, D. S. Wiersma, C. Fort, and M. Inguscio, Phys. Rev. Lett. **95**, 070401 (2005).
[30] F. Jendrzejewski, A. Bernard, K. Muller, P. Cheinet, V. Josse, M. Piraud, L. Pezze, L. Sanchez-Palencia, A. Aspect, and P. Bouyer, Nat. Phys. **8**, 398 (2012).
[31] S. S. Kondov, W. R. McGehee, J. J. Zirbel, and B. DeMarco, Science **334**, 66 (2011).
[32] M. Endres, M. Cheneau, T. Fukuhara, C. Weitenberg, P. Schau, C. Gross, L. Mazza, M. C. Bauls, L. Pollet, I. Bloch, and S. Kuhr, Science **334**, 200 (2011).